Journal of Colloid and Interface Science 418 (2014) 171–177

Contents lists available at ScienceDirect

Journal of Colloid and Interface Science

www.elsevier.com/locate/jcis

Fabrication of hierarchical core–shell Au@ZnO heteroarchitectures initiated by heteroseed assembly for photocatalytic applications

Yao Qin [b,1], Yanjie Zhou [a,1], Jie Li [b], Jie Ma [a], Donglu Shi [b,d], Junhong Chen [a,c,*], Jinhu Yang [b,*]

[a] College of Environmental Science and Engineering, Tongji University, Siping Road 1239, Shanghai 200092, People's Republic of China
[b] Institute for Biomedical Engineering & Nano Science, School of Medicine, Department of Chemistry, Tongji University, Siping Road 1239, Shanghai 200092, People's Republic of China
[c] Department of Mechanical Engineering, University of Wisconsin-Milwaukee, 3200 North Cramer Street, Milwaukee, WI 53211, USA
[d] Materials Science and Engineering Program, Department of Mechanical and Materials Engineering, University of Cincinnati, Cincinnati, OH 45221-0072, USA

ARTICLE INFO

Article history:
Received 3 September 2013
Accepted 4 December 2013
Available online 11 December 2013

Keywords:
Hierarchical
Heterostructures
Core–shell
ZnO nanorod arrays
Au nanoparicles
Photocatalysis

ABSTRACT

Three dimensional dandelion-like hierarchical core–shell Au@ZnO heteroarchitectures with ZnO nanorods grown radially on Au nanoparticle (NP) cores have been successfully prepared with a high yield via a simple solution method involving heteroseed-induced nucleation and subsequent heteroepitaxial growth processes. Briefly, mercaptopropionic acid (MA) modified Au NPs were synthesized beforehand and served as nucleation centers for primary ZnO seed generation and Au@ZnO heteroseed formation. Then an epitaxial growth of ZnO nanorods (ZnO NRs) on the Au@ZnO heteroseeds resulted in the formation of Au@ZnO dandelions. The photocatalytic properties of as-prepared Au@ZnO dandelions were evaluated through rhodamine B (RhB) photodegradation under UV irradiation. The result showed that the Au@ZnO dandelions had improved photocatalytic performance compared with pure ZnO NRs and hybrids of ZnO NRs/Au NPs, due likely to the synergistic effect of the metal–semiconductor heterojunction and the unique dandelion-like hierarchical core–shell structure.

1. Introduction

Semiconductor–metal heterostructured nanomaterials have attracted great interest in recent years because they can not only combine the unique properties of metals and semiconductors, but also generate novel electrical, optical, and catalytic properties due to the synergetic interaction between the metal and the semiconductor components [1–6]. As a representative class of semiconductor–metal nanostructured materials, Au–ZnO nanocomposites have received special attention due to their promising applications in solar energy conversion [7], biological detection [8,9], sensing fields [10–12] as well as photocatalysis [13–16]. Moreover, from the perspective of fundamental science, it is of great significance to explore novel photoelectric mechanisms tied to the morphologies and structures of Au–ZnO heterojunction materials, and their relevant catalytic, optical and electric properties [2,17–22]. Therefore, great efforts have been devoted to fabricating Au–ZnO nanocomposites with different shapes and structures recently. For example, a variety of ZnO–Au heterostructures including ZnO NRs/Au NPs [17,18,22–24], flower-like ZnO/Au NPs [7,10,13–14,25–26], ZnO nanocones/Au NPs [15,27], and ZnO NPs/Au NPs [9,28–32] have been synthesized. However, in most of these work, gold NPs were merely dispersed or deposited on the surface of presynthesized ZnO nanostructures. In contrast, inverse structure form of the two components such as Au@ZnO core–shell structures where ZnO nanostructures grown on Au NPs prepared via reverse synthetic approaches was seldom reported [33–35], due probably to the synthesis difficulty of growing ZnO nanostructures on gold nuclei. Nonetheless, as reported by Xu's group, core–shell structured M@TiO_2 (M = Au, Pd, Pt) nanocomposites encapsulating metal NPs within the semiconductor shell in fact exhibited much higher stabilities against aggregation and undesirable metal corrosion in the practical photocatalysis applications than their oxide supported counterparts [36–37]. Thus, more subtle structure design for Au–ZnO core–shell nanocomposites is highly desired to fully explore their potential advantages as promising heterostructured photocatalysts. It is generally recognized that effective separation and transportation of photogenerated charges as well as high light harvesting of photocatalysts play decisive roles in determining their photocatalytic performance [14,19,38]. Therefore, for Au@ZnO heterostructures to acquire high photocatalytic activity, particular structure designs are required: First, complete separation of Au cores and ZnO shells with defined interfaces. This is beneficial for not only effective electron–hole separation and transfer at the interfaces of the cores and shells, but also the subsequent

* Corresponding authors. Address: Department of Mechanical Engineering, University of Wisconsin-Milwaukee, 3200 North Cramer Street, Milwaukee, WI 53211, USA (J. Chen). Fax: +86 021 65983706 (J. Yang).
E-mail addresses: jhchen@uwm.edu (J. Chen), yangjinhu2010@gmail.com (J. Yang).
[1] These authors contributed equally to this work.

0021-9797/$ - see front matter © 2013 Elsevier Inc. All rights reserved.
http://dx.doi.org/10.1016/j.jcis.2013.12.013

reduction and oxidation half reactions proceeded separately in the core and shell regions [39]. Second, highly epitaxial ZnO nanostructure with high carrier mobility. It can facilitate charge transportation and thus reduce charge recombination. Third, open hierarchical architectures of the Au@ZnO nanocomposites with large specific surface area (SSA). These features will guarantee high light trapping capacity and provide abundant accessible sites for effective molecule adsorption/desorption [38].

Through a rational design, here we demonstrate the fabrication of 3D hierarchical core–shell Au@ZnO dandelions through a simple solution approach involving heteroseed induced nucleation and epitaxial growth of ZnO nanorods. The synthesized product is composed of Au NP cores and ZnO shells of nanorod arrays grown radially on Au cores. The as-prepared Au@ZnO dandelions are attractive for photocatalysis according to the structure advantages discussed above: separate Au and ZnO components confined in respective core and shell regions with good interfacial contact for effective charge separation and transfer at the interface of Au cores and ZnO shells, 1D ZnO nanorods with high carrier mobility for fast and direct electron transportation over all shells, dandelion-like hierarchical architectures with relatively high SSA for efficient light trapping and molecule adsorption/desorption. Besides, radial ZnO nanorod arrays anchored tightly on Au NP cores can avoid serious aggregation relative to common catalysts in the form of dispersed nanoparticles, guaranteeing high catalytic stability and long lifetime of the catalyst. To the best of our knowledge, the novel Au@ZnO dandelions are reported here for the first time. As expected, the typical Au@ZnO dandelions display higher photocatalytic activity and stability when evaluated through RhB photodegradation, compared with other pure ZnO nanorods (ZnO NRs), ZnO nanorod-Au NP hybrid (ZnO NRs–Au NPs, prepared by depositing Au NPs on the surface of ZnO nanorods).

2. Materials and methods

2.1. Materials

Chloroauric acid ($HAuCl_4{\cdot}4H_2O$), Rhodamine B (RhB) and mercaptopropionic acid (MA) were purchased from Alfa Aesar. Anhydrous zinc acetate ($Zn(CH_3COO)_2$) and sodium citrate were purchased from Sigma–Aldrich Company. Hexamethylene tetramine(HMT), potassium hydroxide(KOH) and anhydrous ethanol were purchased from Shanghai Chemical Reagent Co., Ltd. All the above reagents are of analytical grade and used as purchased.

2.2. Synthesis of the Au@ZnO dandelions

Briefly, Au nanoparticles with the size of ~20 nm were synthesized by reduction of chloroauric acid ($HAuCl_4$) using citrate according to Ref. [40] and further modified with MA (see S1.1). Then these MA-capped Au nanoparticles were introduced into the solution for growing ZnO seed nanoparticles to fabricate the Au@ZnO heteroseeds (S1.2). Subsequently, the obtained Au@ZnO heteroseeds were casted into 50 mL aqueous solution composed of equimolar zinc nitrate and hexamethylenetetramine (HMT) at 95 °C for preparation of the Au@ZnO dandelions (S1.3).

2.3. Characterization

Morphology was characterized using a scanning electron microscope (SEM, Hitachi S4800, 3 kV) and high-resolution transmission electron microscopy (HR-TEM, JEM 2011, 200 kV). The crystal structure was determined by X-ray diffraction (XRD) using a D/max2550VB3+/PC X-ray diffractometer with Cu Kα radiation with a 1.5418 Å wavelength. A beam voltage of 40 kV and a 100 mA current beam were used. The UV–vis spectra of the samples were recorded on a Cary-50 UV–vis spectrophotometer. The Zeta potential measurements were recorded on a NanoZS90 (Malvern) particle size analyzer.

2.4. Photocatalytic evaluation

A mixture of 30 mL 1.0×10^{-5} M RhB aqueous solution and 6 mg catalyst powder of the Au@ZnO dandelions or pure ZnO NRs or ZnO NRs–Au NPs were stirred for 1 h in a quartz tube in the dark to reach adsorption equilibrium and then irradiated by a 300 W high-pressure mercury lamp under magnetic stirring in air. Samples of the suspension were draw out at regular intervals, centrifuged to completely remove the catalyst, and then measured using a UV–vis spectrophotometer to detect the degree of RhB degradation.

3. Results

The representative SEM images of the product obtained under standard conditions are shown in Fig. 1a and b. According to Fig. 1a, the product consists of high-yield dandelion-like spherical assemblies with about 1–1.5 μm in size. Fig. 1b is an enlarged SEM image of these dandelion-like assemblies, which suggests that each "dandelion" is comprised of radially arrayed nanorods with 50–100 nm in diameter and 500–700 nm in length growing around a core. The typical TEM image in Fig. 1c further reveals that the core is actually made of loosely aggregated nanoparticles with average diameter of ~20 nm, which is in accord with the size of initially introduced Au NPs, suggesting that Au NP clusters are embedded in the cores after the growth process. It is noteworthy that the Au NPs existing in this embedded manner occupy an overwhelming majority and few bare Au NPs are observed on surfaces of the dandelions. After fierce ultrasonic treatment, a piece of nanorod bundle obtained from the shell layer of a dandelion was selected for closer observation (Fig. 1d, inset). The high-magnification TEM image (Fig. 1d), taken from the circled region on a nanorod of the bundle, displays clearly a set of crystal lattices with *d* spacing of 0.26 nm, corresponding to the {002} planes of the hexagonal structured wurtzite ZnO (JCPDS No. 36-1451), which together with the SAED pattern (Fig. S3) indicates the nanorods are single ZnO crystal with the growth direction of [002]. Further composition analysis of the product is confirmed by corresponding XRD data, as shown and indexed in Fig. 1e, where two sets of prominent diffraction peaks correspond to wurtzite ZnO and cubic-phase Au (JCPDS No. 04-0784), respectively. Therefore, the synthesized dandelion-like product actually has a 3D hierarchical core–shell heteroarchitecture, that is, Au NP cores are covered by ZnO shells consisting of radial nanorod arrays.

4. Discussions

To investigate the formation mechanism of the Au@ZnO dandelions, the morphology evolution of Au NPs at different synthesis stages before and after ZnO seed coating was traced (Fig. 2). Fig. 2a presents the typical Au NPs synthesized according to Frens's method [40]. It can be seen that the gold NPs without ZnO seed coating are monodisperse with a uniform diameter of about 20 nm. The HRTEM image (inset in Fig. 1a) shows several discrete lattice fringes with equal lattice distance of 0.23 nm corresponding to the {111} planes of cubic-phase gold, reflecting the multiple twinned crystal nature of Au NPs. However, after ZnO seed coating, Au NPs become obviously aggregated due to the decrease of electrostatic repulsion between the nanoparticles (Zeta potential changed from −32.9 to −7.76 mV, see Table S1). Further HRTEM

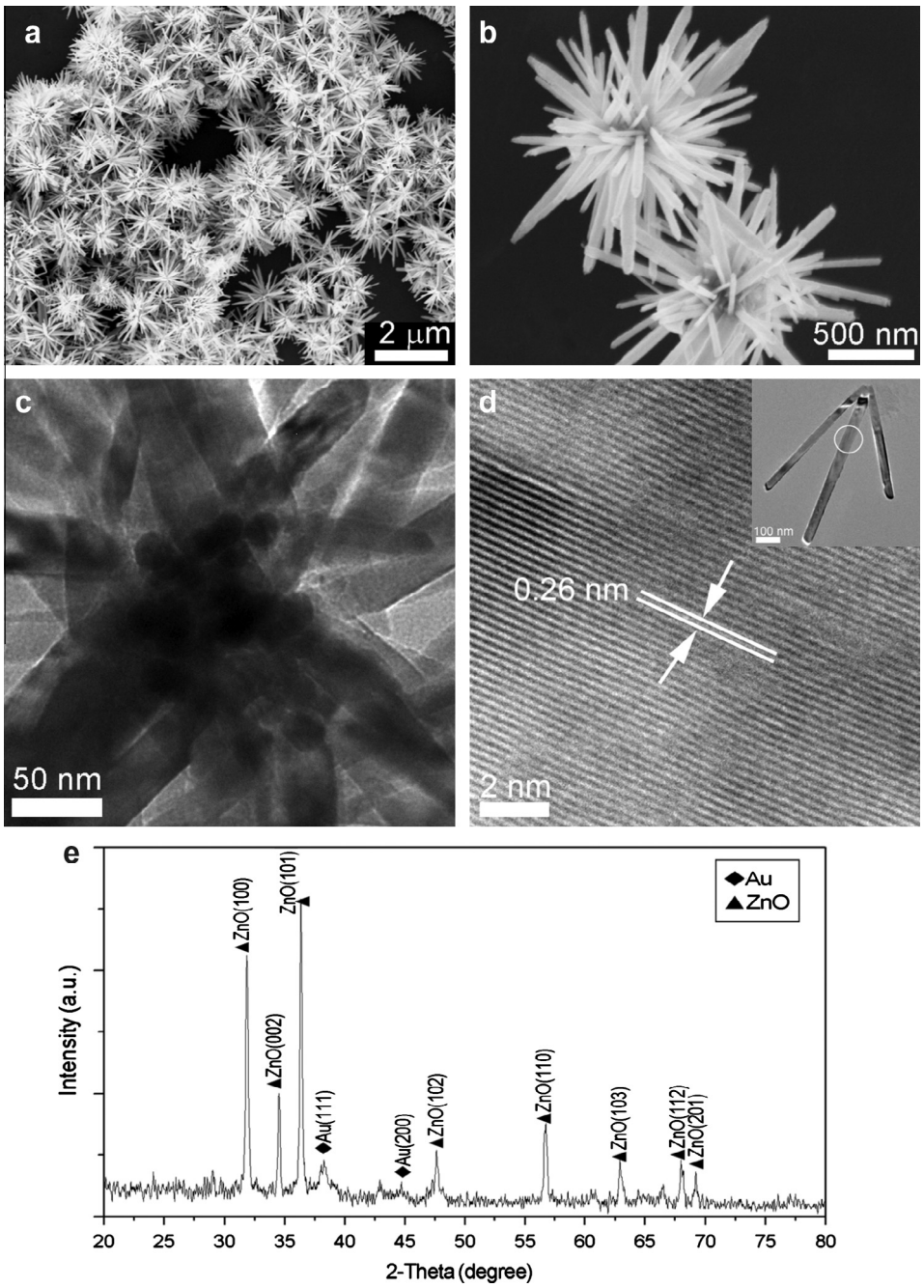

Fig. 1. SEM images (a and b), TEM images (c and d) and XRD pattern (e) of the synthesized Au@ZnO dandelions under standard conditions.

characterization, taken from two squared regions in Fig. 2b, is given in Fig. 2c and d respectively, where several crystallites (denoted with dashed circles) show the respective lattice distances of 0.26 nm and 0.28 nm that agree well with the d spacing of {002} and {100} planes of wurtzite ZnO. This result indicates that the Au NP cores are surrounded by abundant ZnO nanoseeds with size estimated to be several nanometers. On the basis of these Au@ZnO heteroseeds, the Au–ZnO dandelions were obtained in the typical aqueous growth solution containing equimolar zinc nitrate and hexamethylenetetramine (HMT), as shown in Fig. 1a and b.

The Au NP cores and the subsequently introduced ZnO seeds are believed to be both pivotal to forming the hierarchical Au@ZnO dandelions. This is directly supported by the contrast synthetic experiments conducted in the absence of Au NPs or ZnO seeds under otherwise the same typical conditions. As shown in Fig. 3a and Fig. S1b and d, only microsized ZnO polycrystals made mainly of multiple or twin nanorods were produced in the absence of Au NPs at typical or lower ZnO seed concentrations. Also, if without ZnO seeds, only ZnO branched nanorods with very thick trunks (~1 μm) were formed (Fig. 3b). It was found that Au NPs in this case were either attached on the surface of ZnO branched nanorods or existed separately on substrates, which means the nucleation was not occurred on Au NPs without ZnO seed assistance. In fact, ZnO nanorod arrays grown on arbitrary seed-preloaded planar substrates [41,42] or even non-planar substrate such as nanowires in our previous work [38], have been well reported. The key to success is fulfilling effective coating of ZnO seeds on the substrates. Obviously, compared with planar substrates or the non-planar nanowires, the Au NPs in this work with sizes down to 20 nm have ultrahigh curvature and tension, and thereby the successful

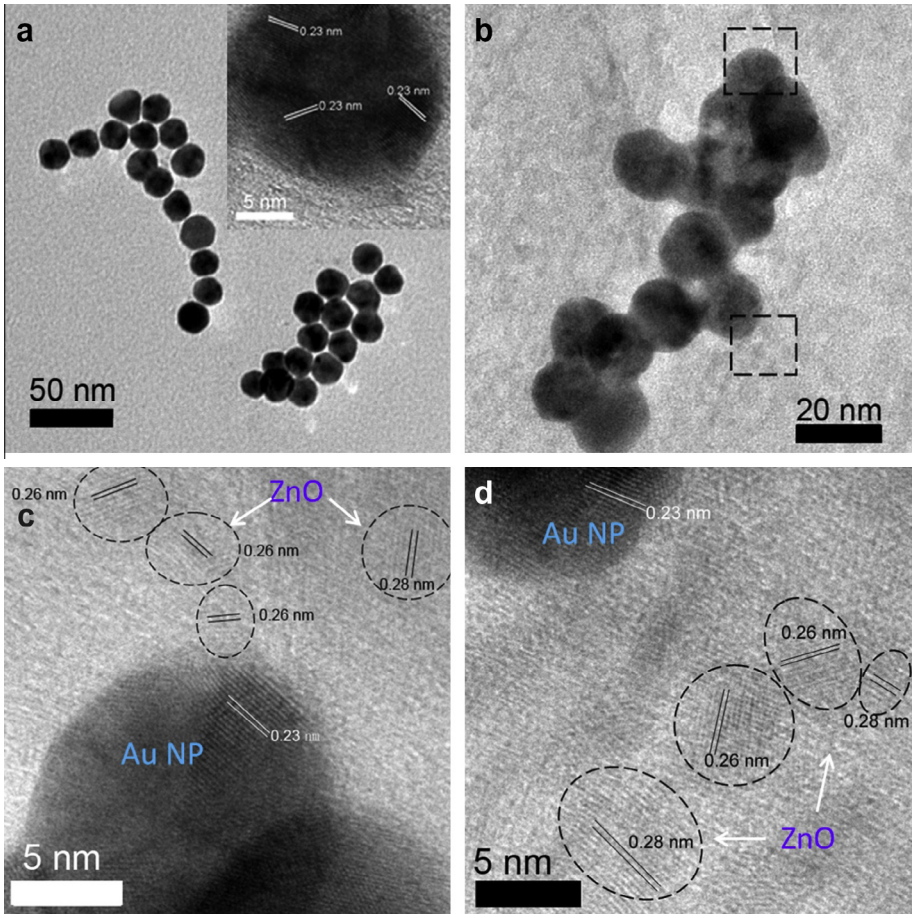

Fig. 2. TEM images of Au nanoparticles before (a) and after (c and d) ZnO seed coating. Inset in (a) is the HRTEM image of a gold seed nanoparticle. Enlarged HRTEM images in (c and d) correspond to the top and bottom right regions denoted with dashed square in (b), respectively.

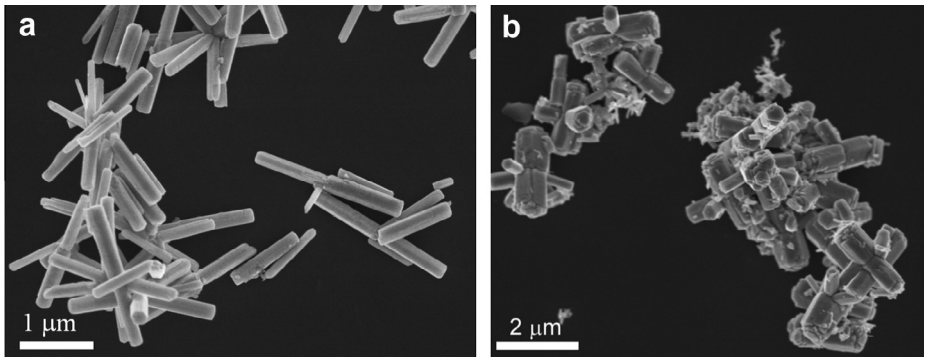

Fig. 3. SEM images of the as-synthesized products synthesized in contrast synthetic experiments under otherwise typical conditions except (a) without gold seeds or (b) without ZnO seeds.

loading of ZnO seeds on their surfaces is a much bigger challenge. We think the MA modification of Au NPs and the selection of Zn source at a proper concentration are key steps for the ZnO seed loading and high-quality Au@ZnO heteroseed formation, while the Au@ZnO heteroseeds are pivotal importance for the generation of the Au@ZnO dandelions.

Therefore, based on the results obtained and discussion above, we propose here a tentative mechanism emphasizing Au@ZnO heteroseed generation through self-assembly and subsequent heteroepitaxial growth for the formation of the Au@ZnO dandelions. As illustrated in Scheme 1, when MA modified Au NPs with good dispersion were injected into the reaction solution containing Zn^{2+} ions for ZnO seed loading, Zn^{2+} ions were first caught around by the negatively charged Au NPs (Zeta potential −32.9 mV, Table S1) due to electrostatic attraction. Accordingly, Zn^{2+} ion loaded Au NPs with positively charged surface (Zeta potential 6.92 mV, Table S1) serve as *in situ* nucleation centers for ZnO seeds to form Au–ZnO primary heteroseeds after addition of KOH (Scheme 1a). However the added excess KOH will gradually neutralize the positive charges of the initially formed Au–ZnO

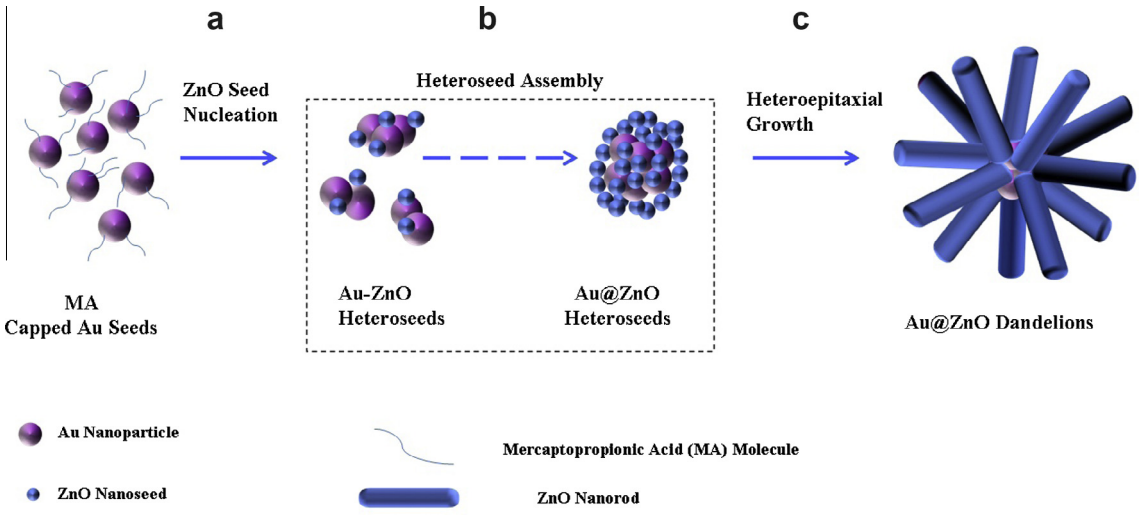

Scheme 1. Schematic illustration of the heteroseed assembly induced formation process of Au@ZnO dandelions.

heteroseeds and further cause their surface charge switch from positive to negative (Zeta potential from 6.92 mV to −7.76 mV, Table S1). This switch accompanying with isoelectric point appearing inevitably leads to spontaneous self-assembly of the primary Au–ZnO heteroseeds to the Au@ZnO core–shell heteroseeds (Scheme 1b). Finally, the Au@ZnO heteroseeds serve as non-planar substrates for the growth of ZnO nanorod arrays and eventually formation of Au@ZnO dandelions (Scheme 1c). It is noted that Au NPs are thought to play two important roles in the assembly process (Scheme 1a and b) and be essential for the synthesis: firstly, Au NPs work as scaffolds carrying the ZnO seeds to form the Au@ZnO heteroseeds, which provides stable core–shell nuclei for the epitaxial growth of ZnO nanorods and final formation of the Au@ZnO dandelions. Secondly, Au NPs also serve as effective substrates to avoid possible severe aggregation of the ZnO seeds, benefiting the subsequent growth of ordered and uniform ZnO nanorods in the shell layer rather than disordered rods formed in the absence of Au NPs (Fig. 3a and Fig. S1b and d).

Photodegradation of rhodamine B (RhB) which is a typical organic azo-dye pollutant in the textile industry is used as a model reaction to evaluate the photocatalytic performances of the synthesized Au@ZnO dandelions in aqueous solution. For comparisons, pure ZnO nanorods (ZnO NRs, see Fig. 3a) and ZnO nanorod–Au NP hybrid (ZnO NRs–Au NPs, see Fig. S2) have also been prepared by similar methods (S2) and investigated with photocatalysis together. Fig. 4a shows the photocatalytic degradation of RhB (10^{-5} M) in aqueous solution under UV irradiation. It can be observed that RhB is completely degraded by 6 mg Au@ZnO dandelions within 40 min. The comparison results of the photocatalytic properties for the Au@ZnO dandelions, the pure ZnO NRs and the ZnO NRs–Au NPs are demonstrated in Fig. 4b. The degradation process approximately complies with the pseudo-first-order kinetics as show in formula (1).

$$\ln\left(\frac{C}{C_0}\right) = -kt \tag{1}$$

here, C_0 and C are the initial concentration of RhB and the corresponding concentration along with the exposure time t, respectively. k is the degradation constant. In the initial 20 min, the calculated k values for Au–ZnO dandelions, ZnO NRs–Au NPs, ZnO NRs and the blank sample are 0.09368, 0.10704, 0.07892 and 0.01131 min^{-1}, respectively. Accordingly, the photocatalytic efficiency in this period follows the order: ZnO NRs–Au NPs > Au@ZnO dandelions > ZnO NRs > blank (i.e., no catalyst added). It is obvious

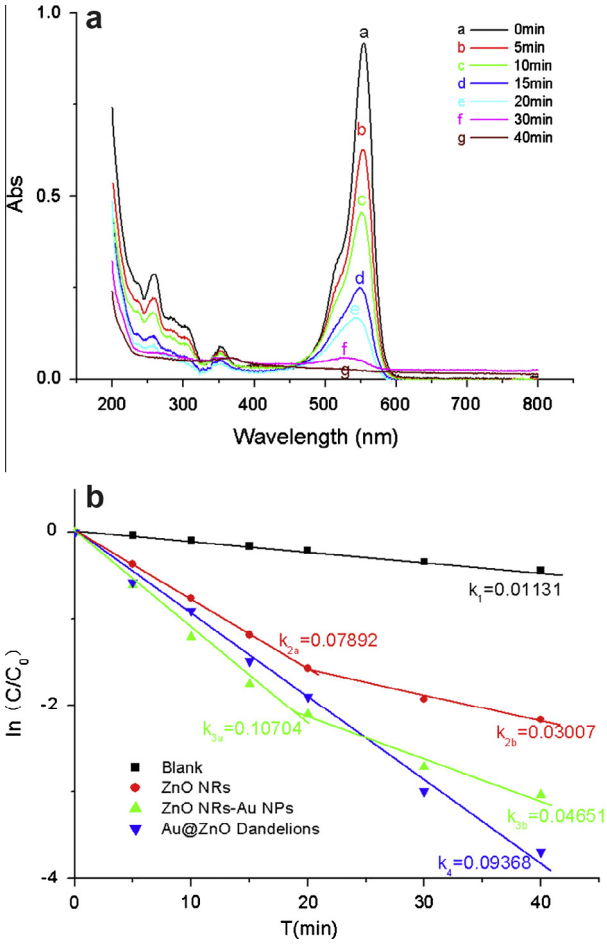

Fig. 4. (a) Absorption spectra of rhodamine B as a function of the degradation time under UV irradiation by using Au@ZnO dandelions as the photocatalyst. (b) Photocatalytic properties of as-prepared Au@ZnO dandelions as well as ZnO NRs–Au NPs, pure ZnO NRs and the blank (without any catalyst added).

that heterostructured catalysts, either the typical Au@ZnO dandelions or ZnO NRs–Au NPs, have improved photocatalytic activity compared with pure ZnO counterparts. The enhanced photocatalytic performance of the Au@ZnO dandelions or ZnO NRs–Au NPs

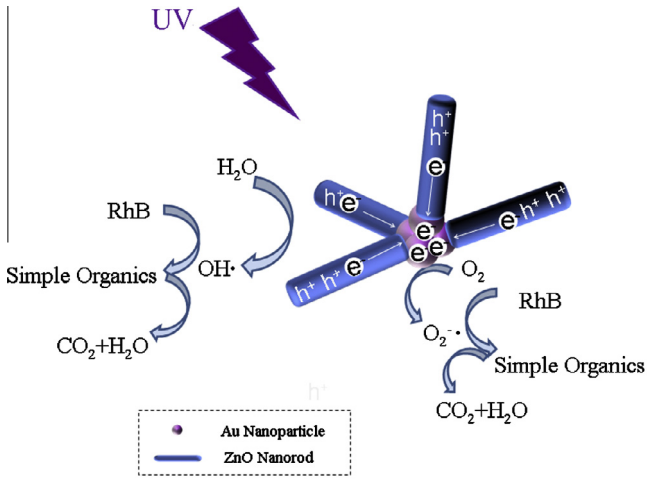

Scheme 2. Schematic illustration of photocatalytic mechanism of the Au@ZnO dandelions.

should be ascribed to the synergistic effect of wide-bandgap semiconductor and noble metal as reported in previous papers [13,15,16,19,30], that is, the heterojunctions facilitate more effective separation of photoinduced electrons and holes and thus reduce the charge recombination significantly due to their equilibrium band structure. Especially for the Au@ZnO dandelions, photogenerated electrons and holes can be stored separately into Au cores and ZnO shells after rapid separation through interface, responsible for high-efficient reduction and oxidation half reactions in respective regions. It is noted that though the ZnO NRs–Au NPs shows even higher photocatalytic efficiency than the Au@ZnO dandelions in the beginning of the catalytic reactions, it gradually lose its photocatalitic activity after 20 min. For example, the average k values for ZnO NRs–Au NPs were decreased by 56% i.e. from 0.10704 min^{-1} to 0.04651 min^{-1} (Fig. 4B), comparing the degradation rates between the first and the second 20 min. The similar catalytic activity decease (61%) was also happened to the pure ZnO NR catalyst which is made of the similar NRs. In contrast, the Au@ZnO dandelions retain their high photocatalytic activity throughout the reaction till RhB is completely degraded. Since both the ZnO NRs–Au NPs and the Au@ZnO dandelions are heterostructured with similar composition, the steadier photocatalytic performance of the latter should arise from its special structure with high stability. Namely, (i) hierarchical architecture, which well keeps the catalyst nanoparticles from aggregation, can prevent the loss of active sites and photogenerated carriers. (ii) Open shell structure, made of the radial nanorod arrays, can facilitate molecule accessibility for full adsorption and desorption before and after degradation, respectively, which favor quick recovery of the active sites. Accordingly, the catalytic mechanism of the Au–ZnO dandelions is shown in Scheme 2. Under UV irradiation, photoelectrons will transfer from the surface of the ZnO nanorod shell to the Au core, leaving a quantity of holes on the ZnO surface. The electron-enriched Au cores as well as the radially distributed ZnO NRs in the shell layer with high carrier transport and rapid molecule diffusion properties actually serve as steady spatial catalyzing centers for efficient RhB molecule degradation [43–45].

5. Conclusions

In summary, we have prepared novel Au@ZnO core–shell dandelions with 3D hierarchical architectures through a solution growth approach initiated by heteroseed assembly and nucleation. Compared with pure ZnO NRs and heterostructured ZnO NRs–Au NPs, the typical Au@ZnO dandelions display higher photocatalytic activity and stability in photodegradation of RhB. The enhanced performance is ascribed to its special core–shell hierarchical heterostructures that are beneficial for photogenerated charge separation, carrier transportation and molecule diffusion. Moreover, the stable structure of the spatially distributed ZnO nanorods in the dandelion shell layer endows the catalyst a steady catalytic activity which is crucial for practical use. In addition, owing to their unique structure, the as-prepared Au@ZnO dandelions with uniform shape and controlled composition are expected to provide new perspectives in various fields such as solar cells, photochemical water splitting, chemical and biological sensors.

Acknowledgments

This work was financially supported by National Natural Science Foundation (21001082, 21273161 and 21101117), Shanghai Innovation program (13ZZ026), Scientific Research Foundation for the Returned Overseas Chinese Scholars of SEM, The Program for Professor of Special Appointment (Eastern Scholar) at Shanghai Institutions of Higher Learning (2013-13), Visiting scholar fund of the Key Laboratory for Ultrafine Materials of Ministry of Education, East China University of Science and Technology, and the Fundamental Research Funds for the Central Universities.

Appendix A. Supplementary material

Detailed Synthesis approaches of the Au@ZnO dandelions (S1.1–S1.3), synthesis of pure ZnO NRs and ZnO NRs–Au NPs (S2), SEM of the products in the presence and absence of Au NPs at lower ZnO seed concentrations (Fig. S1), SEM of the ZnO NRs–Au NPs (Fig. S2) and Zeta potential data of the products at different synthetic stages (Table S1). Supplementary data associated with this article can be found, in the online version, at http://dx.doi.org/10.1016/j.jcis.2013.12.013.

References

[1] A. Dawson, P.V. Kamat, J. Phys. Chem. B 105 (2001) 960–966.
[2] V. Subramanian, E.E. Wolf, P.V. Kamat, J. Phys. Chem. B 107 (2003) 7479–7485.
[3] J.S. Lee, E.V. Shevchenko, D.V. Talapin, J. Am. Chem. Soc. 130 (2008) 9673–9675.
[4] P.V. Kamat, J. Phys. Chem. C 112 (2008) 18737–18753.
[5] R. Costi, G. Cohen, A. Salant, E. Rabani, U. Banin, Nano Lett. 9 (2009) 2031–2039.
[6] D.V. Talapin, J.S. Lee, M.V. Kovalenko, E.V. Shevchenko, Chem. Rev. 110 (2010) 389–458.
[7] V. Dhas, S. Muduli, W. Lee, S.-h. Han, S. Ogale, Appl. Phys. Lett. 93 (2008) 243108 (3 pages).
[8] Y. Liu, M. Zhong, G. Shan, Y. Li, B. Huang, G. Yang, J. Phys. Chem. B 112 (2008) 6484–6489.
[9] G. Shan, S. Wang, X. Fei, Y. Liu, G. Yang, J. Phys. Chem. B 113 (2009) 1468–1472.
[10] X.J. Wang, W. Wang, Y.L. Liu, Sens. Actuat. B-Chem. 168 (2012) 39–45.
[11] L.L. Wang, Z. Lou, T. Fei, T. Zhang, J. Mater. Chem. 22 (2012) 4767–4771.
[12] J. Zhang, X. Liu, S. Wu, B. Cao, S. Zheng, Sens. Actuat. B-Chem. 169 (2012) 61–66.
[13] H. Li, E.T. Liu, F.Y.F. Chan, Z. Lu, R. Chen, Mater. Lett. 65 (2011) 3440–3443.
[14] P.K. Chen, G.J. Lee, S. Anandan, J.J. Wu, Mater. Sci. Eng. B 177 (2012) 190–196.
[15] P. Li, Z. Wei, T. Wu, Q. Peng, Y. Li, J. Am. Chem. Soc. 133 (2011) 5660–5663.
[16] N. Udawatte, M. Lee, J. Kim, D. Lee, ACS Appl. Mater. Interfaces 3 (2011) 4531–4538.
[17] W.Q. Zhang, Y. Lu, T.K. Zhang, W. Xu, M. Zhang, S.H. Yu, J. Phys. Chem. C 112 (2008) 19872–19877.
[18] B. Chen, H. Zhang, N. Du, D. Li, X. Ma, D. Yang, Mater. Res. Bull. 44 (2009) 889–892.
[19] J. Lee, H.S. Shim, M. Lee, J.K. Song, D. Lee, J. Phys. Chem. Lett. 2 (2011) 2840–2845.
[20] B.J. Niu, L.L. Wu, W. Tang, X.T. Zhang, Q.G. Meng, Cryst. Eng. Comm. 13 (2011) 3678–3681.
[21] Z. Mao, W. Song, L. Chen, W. Ji, X. Xue, W. Ruan, Z. Li, H. Mao, S. Ma, J.R. Lombardi, B. Zhao, J. Phys. Chem. 115 (2011) 18378–18383.
[22] S.T. Kochuveedu, J.H. Oh, Y.R. Do, D.H. Kim, Chem. Eur. J. 18 (2012) 7467–7472.
[23] H. He, W. Cai, Y. Lin, B. Chen, Langmuir 26 (2010) 8925–8932.

[24] E. Castillejos, R. Bacsa, A. Guerrero-Ruiz, I. Rodriguez-Ramos, L. Datas, P. Serp, Nanoscale 3 (2011) 929–932.
[25] M. Ahmad, Y.Y. Shi, A. Nisar, H. Sun, W. Shen, J. Zhu, J. Mater. Chem. 21 (2011) 7723–7729.
[26] C. Xiang, Y. Zou, L.-X. Sun, F. Xu, Sens. Actuat. B-Chem. 136 (2009) 158–162.
[27] N.P. Herring, K. Abouzeid, M.B. Mohamed, J. Pinsk, M.S. El-shall, Langmuir 27 (2011) 15146–15154.
[28] J. Strunk, K. Ka, X.Y. Xia, M. Comotti, F. Schuth, T. Reinecke, M. Muhler, Appl. Catal. A: Gen. 359 (2009) 121–128.
[29] H. Wu, L. Wang, J. Zhang, Z. Shen, J. Zhao, Catal. Commun. 12 (2011) 859–865.
[30] S. Sarkar, A. Makhal, T. Bora, S. Baruah, Phys. Chem. Chem. Phys. 13 (2011) 12488–12496.
[31] X. Wang, X. Kong, Y. Yu, H. Zhang, J. Phys. Chem. C 111 (2007) 3836–3841.
[32] X. Han, W.J. Qin, J. Sun, J. Yang, K.Y. Niu, H.L. Wang, X.W. Du, Mater. Lett. 63 (2009) 1093–1095.
[33] K.K. Haldar, T. Sen, A. Patra, J. Phys. Chem. C 112 (2008) 11650–11656.
[34] L. Sun, G. Wei, Y. Song, Z. Liu, L. Wang, Z. Li, Mater. Lett. 60 (2006) 1291–1295.
[35] X. Han, W.J. Qin, J. Sun, J. Yang, K.Y. Niu, H.L. Wang, X.W. Du, J. Alloy. Compd. 477 (2009) 661–664.
[36] N. Zhang, S.Q. Liu, X.Z. Fu, Y.J. Xu, J. Phys. Chem. C 115 (2011) 9136–9145.
[37] N. Zhang, S. Liu, Y.J. Xu, Nanoscale 4 (2012) 2227–2238.
[38] S.W. Wang, Y. Yu, Y.H. Zuo, C.Z. Li, J.H. Yang, C.H. Lu, Nanoscale 4 (2012) 5895–5901.
[39] T. Hirakawa, P.V. Kamat, J. Am. Chem. Soc. 127 (2005) 3928–3934.
[40] G. Frens, Nat. Phys. Sci. 241 (1973) 20–22.
[41] L.E. Greene, M. Law, J. Goldberger, F. Kim, J.C. Johnson, Y.F. Zhang, R.J. Saykally, P.D. Yang, Angew. Chem. Int. Ed. 42 (2003) 3031–3034.
[42] L.E. Greene, M. Law, D.H. Tan, M. Montano, J. Goldberger, G. Somorjai, P.D. Yang, Nano Lett. 5 (2005) 1231–1236.
[43] C.C. Chen, W.H. Ma, J.C. Zhao, Chem. Soc. Rev. 39 (2010) 4206–4219.
[44] J.Y. Li, W.H. Ma, P.X. Lei, J.C. Zhao, J. Environ. Sci. 19 (2007) 892–896.
[45] J.Y. Li, W.H. Ma, C.C. Chen, J.C. Zhao, H.Y. Zhu, X.P. Gao, J. Molecular Catal. A: Chem. 261 (2007) 131–138.